

The Masses of the Orion Proplyds from Submillimeter Dust Emission

Jonathan P. Williams and Sean M. Andrews

*Institute for Astronomy, 2680 Woodlawn Drive, Honolulu, HI 96822; jpw@ifh.hawaii.edu,
andrews@ifh.hawaii.edu*

and

David J. Wilner

*Harvard-Smithsonian Center for Astrophysics, 60 Garden Street, Cambridge, MA 02138;
dwilner@cfa.harvard.edu*

ABSTRACT

We have imaged the 880 μm continuum emission from the “proplyds” in the center of the Trapezium Cluster in Orion using the Submillimeter Array with a beam size $1''.5$ FWHM and an rms of 2.7 mJy. Five sources are detected with fluxes in the range 18 to 38 mJy, which includes dust emission from four proplyds and ionized gas from θ^1 Ori G. The total masses of the detected proplyds derived from their dust emission range from 1.3 to $2.4 \times 10^{-2} M_{\odot}$ assuming a dust temperature of 20 K and mass opacity of $0.03 \text{ cm}^2 \text{ g}^{-1}$. Eighteen other proplyds within the field of view are not detected individually, but the flux distribution toward their locations is slightly higher than the background and has an average value of 1.1 mJy which corresponds to a mass of $8 \times 10^{-4} M_{\odot}$. The four detected proplyds have sufficient disk mass bound to their central stars to form planetary systems on the scale of our Solar System.

Subject headings: ISM: individual(Trapezium Cluster, Orion Nebula) — stars: protoplanetary disks — stars: formation

1. Introduction

High mass stars, on account of their luminosities, temperatures and explosive ends, have a disproportionally large effect on the interstellar medium relative to their numbers. Their influence appears to extend down to the scales of star-forming cores and even planet-forming disks. Star formation may be triggered by supernovae shock waves in neighboring clouds

(Elmegreen & Lada 1977) but, at closer quarters, it may be stunted by photoionization and evaporation of molecular clumps within HII regions (Hester et al. 1996). The dramatic *Hubble Space Telescope (HST)* images of photoevaporating protoplanetary disks, or proplyds, in the Orion Nebula beginning with O’Dell, Wen & Hu (1993) indicate that planet formation may, too, be inhibited. Given that most low-mass stars are born in OB associations (McKee & Williams 1997), it is important to study disk evolution in such harsh environments.

The Trapezium Cluster in Orion is the nearest young, massive star forming region and it is consequently the most intensively studied (e.g. O’Dell 2001). Approximately 1200 young stars with ages ~ 1 Myr have been identified toward the central 1 pc diameter of the cluster core (Hillenbrand 1997). A single star of spectral type O6ep, θ^1 Ori C, dominates the ultraviolet radiation field and ionizes the gas cocoons around nearby low-mass stars. The ionized gas is unbound and evaporates from the stars. Mass loss rates averaging $\sim 10^{-7} M_{\odot} \text{ yr}^{-1}$ were first inferred from centimeter wavelength observations by Churchwell et al. (1987). The aforementioned HST data showed that many of the ionized knots are tadpole-shaped structures with a tail extending away from θ^1 Ori C (O’Dell et al. 1993), and near-infrared imaging revealed low-mass stars at their centers (McCaughrean & Stauffer 1994). The visibility of the central stars despite the inferred large mass of circumstellar material led all of these authors to suggest that the ionized gas originates from the surfaces of externally photoionized protoplanetary disks.

As the integrated mass loss of a proplyd over the age of the cluster is larger than typical disk masses around T Tauri stars, it was immediately apparent that their evolution was largely being dictated by their environment. The disk mass that remained, however, could not be determined from the observations. A lower limit can be obtained for the those objects that are seen in silhouette against the bright nebular background but are sufficiently far enough away from θ^1 Ori C that they are not strongly ionized and do not produce significant optical emission (O’Dell & Wen 1994; McCaughrean & O’Dell 1996; Smith et al. 2005). Based on its resolved size and a minimum column density to block the background light, McCaughrean et al. (1998) determined a lower limit to the mass of the giant proplyd 114-426 of $5 \times 10^{-4} M_{\odot} \simeq 0.5 M_{Jupiter}$. This is twenty times lower than the $0.01 M_{\odot}$ minimum formation mass of our Solar System (Weidenschilling 1977) and it is unclear, therefore, whether the proplyds are viable candidates for planet formation on scales of our own Solar System.

Disk masses are best measured at longer wavelengths where the dust emission becomes optically thin. Interferometry is essential to resolve the tightly clustered proplyds from each other and also to filter out the strong emission from the background molecular cloud. Mundy, Looney, & Lada (1995) used the BIMA interferometer at $\lambda 3.5$ mm to image a field around θ^1 Ori C containing 33 proplyds. Several significant peaks were found, four coincident with

proplyds, but the intensity was consistent with free-free emission from ionized gas and they were unable to measure masses. By analyzing the non-detections, however, they were able to place a statistical upper limit of $0.03 M_{\odot}$ on the average disk mass. The dust emission increases at shorter wavelengths and the free-free emission decreases. Using the OVRO array, Bally et al. (1998a) imaged two fields containing a total of six proplyds at $\lambda 1.3$ mm, made a tentative detection of one object and placed upper limits of $0.015 M_{\odot}$ on the other objects. Lada (1999) presented a mosaic of two fields at $\lambda 1.3$ mm with the Plateau de Bure interferometer that claimed three detections. The implied masses were $\sim 0.01 M_{\odot}$ but these have not been analyzed in detail.

The Submillimeter Array¹ (SMA; Ho et al. 2004) is ideally suited to a renewed look at this issue. Located on Mauna Kea, it can operate at shorter wavelengths than other interferometers and is therefore very sensitive to dust emission. Furthermore, it has a relatively large field of view which allows many proplyds to be imaged simultaneously. In this *Letter*, we present SMA observations at $880 \mu\text{m}$ of a single $32''$ full width half maximum (FWHM) field of view toward 23 proplyds around θ^1 Ori C. We detect five sources and measure the average flux for the rest. The observations are described in §2, our results are presented in §3, and we discuss the implications for planet formation in §4.

2. Observations

A single field containing 23 proplyds around θ^1 Ori C was imaged with the SMA using six antennae in its compact configuration on November 13 and 14, 2004. The phase center of the observations was $\alpha(2000) = 5^{\text{h}}35^{\text{m}}16^{\text{s}}.6$, $\delta(2000) = -5^{\circ}23'28''.1$, slightly south-west of θ^1 Ori C to maximize the number of proplyds in the field. The receivers were tuned in double sideband mode to place the CO(3–2) line in the center of the upper sideband. Each sideband provided the correlator with a 2 GHz spectral region separated from the central frequency of 340.7 GHz ($880 \mu\text{m}$) by ± 5 GHz. Weather conditions were very good, and system temperatures varied from 300 to 700 K over different baselines as the field moved from 30° to 65° elevation.

The amplitude and phase were monitored by alternately interleaving 5-minute integrations of the quasars J0423-013 and J0609-157 with each 20 minute observation on source. The stronger J0423-013 was used to perform the final calibration, and J0609-157 was im-

¹The Submillimeter Array is a joint project between the Smithsonian Astrophysical Observatory and the Academia Sinica Institute of Astronomy and Astrophysics, and is funded by the Smithsonian Institution and the Academia Sinica.

aged as a check on the system performance. The bandpass response and flux scaling were determined from a 30 minute observation of Uranus toward the end of each track.

The data for each night were calibrated with the MIR software package. The atmosphere was very stable during both nights and the rms phase error after calibration was $\sim 10^\circ$ on short baselines increasing to $\sim 20^\circ$ on the longer baselines. The passband, gain, and flux calibrated data from each night were then combined during the imaging process in MIRIAD. The total integration time on the θ^1 Ori C field was 9.6 hours. Strong CO emission was detected and the continuum data were extracted by summing over the line free channels.

The shortest projected baseline was $b_{min} = 16 \text{ k}\lambda$ and the observations are therefore largely insensitive to features with angular scales greater than $\lambda/2b_{min} \simeq 13''$ (Wilner & Welch 1994). This greatly reduces the potential confusion of extended emission from the background molecular cloud (Johnstone & Bally 1999).

Inversion of the continuum data to create a “dirty map” showed a strong source near the edge of the field of view at the $\sim 20\%$ gain of the primary beam, coincident with the proplyd 159–350 using the nomenclature of O’Dell & Wen (1994). This source produced artifacts in the southeast part of the map that proved difficult to clean, and we therefore removed a point source at its location from the visibilities before inverting and cleaning to analyze the other sources in the field. The cleanest map and lowest rms in the central region was obtained by removing a 45 mJy source but the source properties derived so far outside the primary beam half power point are highly uncertain. Natural weighting of the uv -data resulted in a beamsize of $1''.9 \times 1''.2$ at position angle 303° east of north and the cleaned map that is presented here was restored with a circular $1''.5$ beam that has the same area as the naturally weighted beam. The rms noise level is $\sigma = 2.7 \text{ mJy beam}^{-1}$.

3. Results

Contours of the continuum emission are shown in Figure 1. The lefthand image shows the location of the four Trapezium O stars and optically identified proplyds relative to the data. The righthand image shows the contours overlaid on the HST image from Bally et al. (1998b) and shows the morphologies, brightness and colors of the proplyds. Five proplyds were detected within the $32''$ FWHM of the primary beam with a peak flux greater than $3\sigma = 8.1 \text{ mJy beam}^{-1}$ and are marked with a red cross in the lefthand image of Figure 1. The two brightest sources, 163-317 and 170-337, were seen in subsets of the data, both lower and upper sidebands, and both the first and second day of observations.

Integrated fluxes for the five sources were measured by summing the pixels within the 3σ contour level and correcting for primary beam attenuation. The emission from 170-337 and

171-340 are merged and the flux for each one was estimated by cutting across the 3σ contour by eye. Most of the proplyds in the field of view were detected at centimeter wavelengths with the VLA (Churchwell et al. 1987; Felli et al. 1993) and have spectral energy distributions that are consistent with thermal bremsstrahlung (Garay, Moran, & Reid 1987). None of the sources that we have detected are variable at 3.6 cm (Zapata et al. 2004), suggesting that any contribution from gyrosynchrotron emission is small and that we are not seeing a bright flare.

Thermal bremsstrahlung emission decreases gradually toward shorter wavelengths but dust emission sharply increases. Spectral energy distributions (SEDs) for the five SMA detections are plotted in Figure 2. A combination of bremsstrahlung and modified ($\beta = 1$) blackbody emission are overlaid. These fits are poorly constrained due to the small number of data points where the SED slopes are changing. Nevertheless, they are adequate to show that the $880\ \mu\text{m}$ flux is dominated by dust emission in all but one case, 167-317, and to estimate the contribution from ionized gas emission in the other four. The measured SMA fluxes, corrected for primary beam attenuation, the peak signal-to-noise ratio, and estimated contribution from bremsstrahlung emission are listed in Table 1.

167-317 (θ^1 Ori G) is the brightest proplyd at centimeter wavelengths and in the Mundy et al. 3.4 mm map. The ionized gas emission is strong even at $880\ \mu\text{m}$ and our SED fit shows that the dust emission contributes only 4.6 mJy to the measured flux. There is some scatter in the centimeter fluxes and a 20% uncertainty in the millimeter fluxes, however, so this number is uncertain. Nevertheless, it does not appear to be a significant detection of dust emission. For the other four sources, however, there is a clear dust excess which allow us to measure the proplyd masses for the first time.

Masses were calculated from the dust excess flux at $880\ \mu\text{m}$ in the standard way way using a distance to Orion of 450 pc and the same Hildebrand (1983) formulation for the grain opacity $\kappa_\nu = 0.1(\nu/1200\ \text{GHz})$ as in Mundy et al. (1995) and Bally et al. (1998a). Implicit in this value is a gas-to-dust ratio of 100 and assumptions about the grain properties. These are discussed further in §4. We assumed a lower temperature, 20 K, than previous work based on the average for disks in Taurus-Auriga (Andrews & Williams 2005) and because the bulk of the disk dust mass lies in the midplane and is shielded from UV-heating even in the intense radiation field at the center of the Trapezium Cluster (Chiang & Goldreich 1997). Masses would be lower by a factor of 3.3 if the dust temperature were 50 K.

Eighteen proplyds are undetected within the primary beam FWHM. As with the previous interferometer observations of the proplyds (Mundy et al. 1995; Bally et al. 1998a), we can study the statistics of the non-detections to constrain their collective properties. The histogram of fluxes in beam-sized apertures around these 18 proplyds is compared to the

background in Figure 2. For this comparison, a region around each of the five detections was blanked out. The flux distribution toward the proplyds is offset from that of the background and has a mean of $0.8 \text{ mJy beam}^{-1}$. This is only a marginally significant result, however, as the map is oversampled. The expected noise in the combination of 18 positions is $2.7/\sqrt{18} = 0.6 \text{ mJy beam}^{-1}$ and the histogram mean is only slightly greater than this. Nevertheless, taken at face value and applying a correction for the mean gain, 0.73, of the interferometer toward the 18 positions, the intrinsic mean flux of the non-detections is 1.1 mJy , which corresponds to a mass of $8 \times 10^{-4} M_{\odot}$.

The integrated CO map showed several resolved clumps of emission but they did not appear coherent in velocity or centered on any of the proplyds. The CO line is optically thick and traces the gas temperature. The temperature probably varies more than the column density in the background cloud and the interferometer map is likely picking up hot spots in the molecular cloud-HII region interface rather than the proplyds themselves.

4. Discussion

These observations have proven more successful at measuring the masses of the Orion proplyds than previous interferometer work because we were able to observe at shorter wavelengths and at higher sensitivity. Our $3\sigma = 8.1 \text{ mJy beam}^{-1}$ detection limit corresponds to a mass limit of $5.6 \times 10^{-3} M_{\odot}$ for individual sources. Allowing for the different dust temperature assumptions, this is an order of magnitude more sensitive than Bally et al. (1998a) who were in turn an order of magnitude more sensitive than Mundy et al. (1995). The IRAM Plateau de Bure map shown in Lada (1999) covers many of the same objects and includes detections of 170-337, 171-340, and 158-327, though the latter detection is not confirmed in our map.

The 23 proplyds within the primary beam FWHM of our map are listed along with their morphological type, projected distance from $\theta^1 \text{ Ori C}$, associated stellar mass, and disk radius in Table 2. The morphology and association with a microjet are taken from the tables in Bally et al. (1998b, 2000). Distances and disk radii are also measured from the HST images in Bally et al. (1998b). Stellar masses are estimated from K-band magnitudes and placement on evolutionary tracks for ages of 0.3 and 1 Myr by McCaughrean & Stauffer (1994).

The statistics are meager, but the four dust detections do not have a preferred morphological type and lie at a range of projected distances. The stellar masses are somewhat uncertain in absolute terms though probably good relative measures and suggest that the detected disks are associated with the more massive (spectral type G to A) stars.

The conversion from submillimeter flux to disk mass contains many uncertainties in the grain properties and gas-to-dust ratio that are encapsulated in the parameter κ . The Hildebrand (1983) formulation that we have used assumes an average grain size of $0.1 \mu\text{m}$, appropriate to interstellar clouds and is normalized to a gas-to-dust ratio of 100. Shuping et al. (2003) show that the typical grain sizes in the outer parts of the giant silhouette proplyd, 114-426, are $\sim 2 - 5 \mu\text{m}$. If the grains are spherical, this does not greatly change the value of κ at 1 mm (Pollack et al. 1994). However, if the grains have aggregated in a fractal manner, the cross-section per unit grain mass may be as much as an order of magnitude higher (Wright 1987) and our proplyd mass estimate may be substantially overestimated. On the other hand, masses would be underestimated if there is dust settling to the disk midplane and grain growth to centimeter sizes and larger (Weidenschilling 1977) or if the inner disk is optically thick (Andrews & Williams 2005).

The gas-to-dust ratio is also highly uncertain. Dust settling to the disk midplane and photoevaporation of the gaseous upper envelopes to the disk will tend to decrease the gas-to-dust ratio below the canonical ISM value of 100 (Throop & Bally 2005) leading to an overestimate of the mass using the Hildebrand κ . We did not clearly detect CO emission from any of the proplyds but future observations of other gas tracers that do not deplete and are abundant in the cold, dense disk midplane will help reveal the gas content and dynamics of the disks.

Given the uncertainty in the mass calculations, it is instructive to compare the submillimeter fluxes from the proplyds with isolated disks in Taurus. After correcting for the greater distance to Orion, the proplyd flux distribution is found to more closely match Taurus Class II than Class I objects (Andrews & Williams 2005). As proplyds lack outer envelopes, this is also their closest morphological match. In this sense, and only for the four dust detections, the Trapezium Cluster environment appears not to have had a substantial effect on these systems.

The stars within the proplyds have ages $\sim 1 \text{ Myr}$ (Hillenbrand 1997) but the evaporation timescales, equal to the disk masses measured here divided by the mass loss rates measured by Churchwell et al. (1987), are of order $10^{-2} M_{\odot}/10^{-7} M_{\odot} \text{ yr}^{-1} \sim 10^5 \text{ yr}$. Note that if disks were originally more massive, they would have been larger in size and their mass loss rates consequently greater. Thus, the present disk mass divided by the present mass loss rate is a good measure of the proplyd lifetime (Störzer & Hollenbach 1999). The resulting discrepancy in timescales may be due to a younger age, $\sim 10^5 \text{ yr}$, for the ionizing source, $\theta^1 \text{ Ori C}$, than the rest of the cluster (Johnstone, Hollenbach, & Bally 1998) or a lower average mass loss rate if either the ionized gas recombines before leaving the system (O’Dell 1998) or if the proplyds move on radial, rather than circular, orbits through the cluster (Störzer & Hollenbach 1999).

In this regard, it is intriguing to note that three of the four dust detections were at a signal-to-noise ratio greater than 7, and one at a signal-to-noise ratio of 4. A smooth distribution of disk masses with increasing numbers at smaller masses should have resulted in proportionally more detections at lower signal-to-noise. The number of detections is small but hints at an abrupt mass loss event such as might be expected for close encounters to θ^1 Ori C on plunging orbits through the cluster. Observations of additional proplyds at a range of distances from θ^1 Ori C will show the disk mass distribution and the effect of environment more clearly. If a distance dependent effect is seen, it would suggest that most stars move on approximately circular orbits and the influence on θ^1 Ori C on planet formation is limited. If the detection rate does not increase with distance, however, it may be that the orbits are eccentric and that θ^1 Ori C would then influence large numbers of potential planetary systems as they pass through the center of the cluster. The effect may be purely destructive through almost complete photoevaporation of a disk but it may also promote the formation of planets via preferential removal of the gas which allows dust disk instabilities to develop (Throop & Bally 2005).

The four dust detections have disk masses slightly greater than the $0.01 M_{\odot}$ minimum mass solar nebula (Weidenschilling 1977). The mass loss is concentrated in the outer parts of the disks where the gravitational potential of the central star is weakest and photoevaporation is most effective (Hollenbach, Yorke, & Johnstone 2000). The radius of the bound inner region depends on the stellar mass and whether the gas is ionized by EUV photons or remains neutral and only heated by the FUV radiation field. The detected proplyds lie far enough away from θ^1 Ori C for the second condition to apply and the central $\sim 20 - 50$ AU radius of the disks survive if the central stellar mass is $1 M_{\odot}$ (Johnstone et al. 1998). Disk radii were measured to be 40 AU in 170–337 and 171–341 (Bally et al. 1998b). Thus, at most, the outer 50% of their disks will be lost and for a surface density $\Sigma \sim r^{-3/2}$, the surviving mass fraction is at least $\sim 60\%$. The other two objects probably have smaller disk radii in which case even more of the mass will survive. We conclude that for these four proplyds, at least, the submillimeter emission indicates there is sufficient material bound to the stars to form Solar System scale planetary systems.

We thank the referee, Mark McCaughrean, for his thorough review which helped improve the paper. Thanks also to Dave Hollenbach, John Bally, and Michael Liu for useful discussions and the SMA staff for carrying out the observations. We acknowledge support from NSF grant AST-0324328 (JPW) and NASA Origins of Solar Systems Program Grant NAG5-11777 (DJW).

5. References

- Andrews, S. M., & Williams, J. P. 2005, ApJ, submitted
- Bally, J., Testi, L., Sargent, A., & Carlstrom, J. 1998a, AJ, 116, 854
- Bally, J., Sutherland, R. S., Devine, D., & Johnstone, D. 1998b, AJ, 116, 293
- Bally, J., O’Dell, C. R., & McCaughrean, M. J. 2000, AJ, 119, 2919
- Chiang, E. I., & Goldreich, P. 1997, ApJ, 490, 368
- Churchwell, E., Wood, D. O. S., Felli, M., & Massi, M. 1987, ApJ, 321, 516
- Elmegreen, B. G., & Lada, C. J. 1977, ApJ, 214, 725
- Felli, M., Churchwell, E., Wilson, T. L., & Taylor, G. B. 1993, A&AS, 98, 137
- Garay, G., Moran, J. M., & Reid, M. J. 1987, ApJ, 314, 535
- Hester, J. J., et al. 1996, AJ, 111, 2349
- Hildebrand, R. H. 1983, QJRAS, 24, 267
- Hillenbrand, L. A. 1997, AJ, 113, 1733
- Ho, P. T. P., Moran, J. M., & Lo, K. Y. 2004, ApJ, 616, L1
- Hollenbach, D. J., Yorke, H. W., & Johnstone, D. 2000, Protostars and Planets IV, 401
- Johnstone, D., Hollenbach, D., & Bally, J. 1998, ApJ, 499, 758
- Johnstone, D., & Bally, J. 1999, ApJ, 510, L49
- Lada, E. A. 1999, NATO ASIC Proc. 540: The Origin of Stars and Planetary Systems, 441
- McCaughrean, M. J., et al. 1998, ApJ, 492, L157
- McCaughrean, M. J., & Stauffer, J. R. 1994, AJ, 108, 1382
- McCaughrean, M. J., & O’Dell, C. R. 1996, AJ, 111, 1977
- McKee, C. F., & Williams, J. P. 1997, ApJ, 476, 144
- Mundy, L. G., Looney, L. W., & Lada, E. A. 1995, ApJ, 452, L137
- O’Dell, C. R., & Wen, Z. 1994, ApJ, 436, 194
- O’Dell, C. R., Wen, Z., & Hu, X. 1993, ApJ, 410, 696
- O’Dell, C. R. 1998, AJ, 115, 263
- Pollack, J. B., Hollenbach, D., Beckwith, S., Simonelli, D. P., Roush, T., & Fong, W. 1994, ApJ, 421, 615
- Shuping, R. Y., Bally, J., Morris, M., & Throop, H. 2003, ApJ, 587, L109
- Smith, N., Bally, J., Licht, D., & Walawender, J. 2005, AJ, 129, 382
- Störzer, H., & Hollenbach, D. 1999, ApJ, 515, 669
- Throop, H. B., & Bally, J. 2005, ApJ, 623, L149
- Weidenschilling, S. J. 1977, Ap&SS, 51, 153
- Wilner, D. J., & Welch, W. J. 1994, ApJ, 427, 898
- Wright, E. L. 1987, ApJ, 320, 818
- Zapata, L. A., Rodríguez, L. F., Kurtz, S. E., & O’Dell, C. R. 2004, AJ, 127, 2252

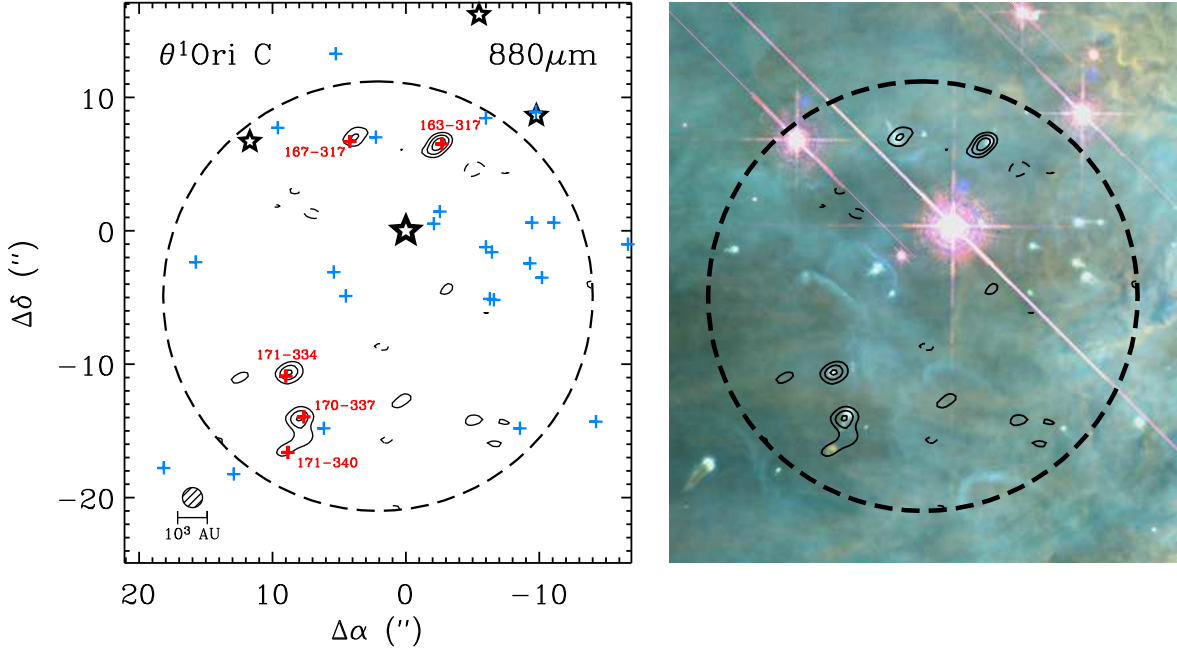


Figure 1: Contours of $880\ \mu\text{m}$ continuum emission toward the proplyds in the Trapezium Cluster. The lefthand image shows the locations of the proplyds; red crosses for the 5 detections labeled with the O’Dell & Wen nomenclature and blue crosses for the 18 non-detections. The position of the four Trapezium O stars are shown by the large star symbols and the center of the coordinate grid has been set to $\theta^1\text{Ori C}$. The $1''.5$ synthesized beam and scale bar are shown in the lower left corner. The contour levels are $3, 5, 7 \times \sigma$ where $\sigma = 2.7\ \text{mJy beam}^{-1}$ is the rms noise level in the map. The righthand image shows the same contours overlaid on the HST image from Bally et al. (1998b). In both images, the large dashed circle shows the FWHM of the primary beam,

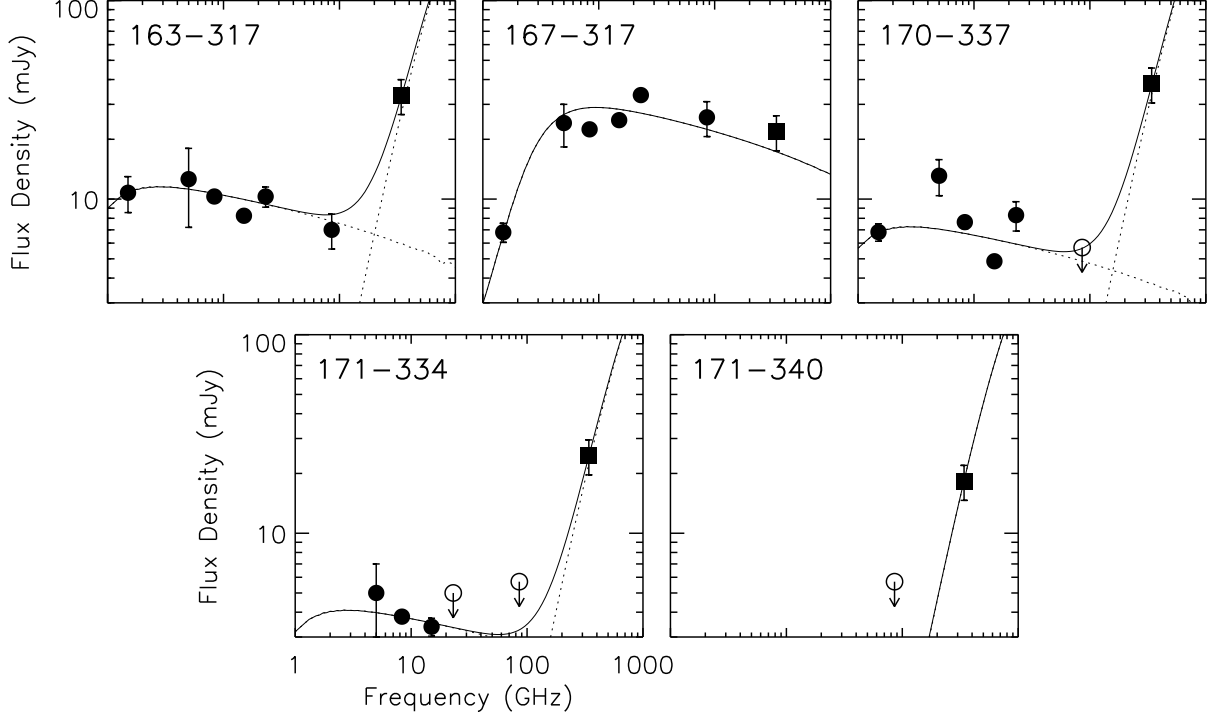


Figure 2: Spectral energy distributions from 20 cm to 880 μm for the five SMA detections. The fluxes shortward of 30 GHz are from VLA observations by Felli et al. (1993), Garay et al. (1987) and Zapata et al. (1994). In the case of multi-epoch observations, the error bar shows the range of measured values. The 86 GHz fluxes are from BIMA observations by Mundy et al. and is estimated for 163-317 from the 3σ contour in their map. Upper limits are shown by open symbols. The squares show the 341 GHz SMA measurements. The uncertainties in the BIMA and SMA measurements are dominated by uncertainties in the flux scales, estimated to 20%. Fits to the ionized gas and dust emission are overlaid.

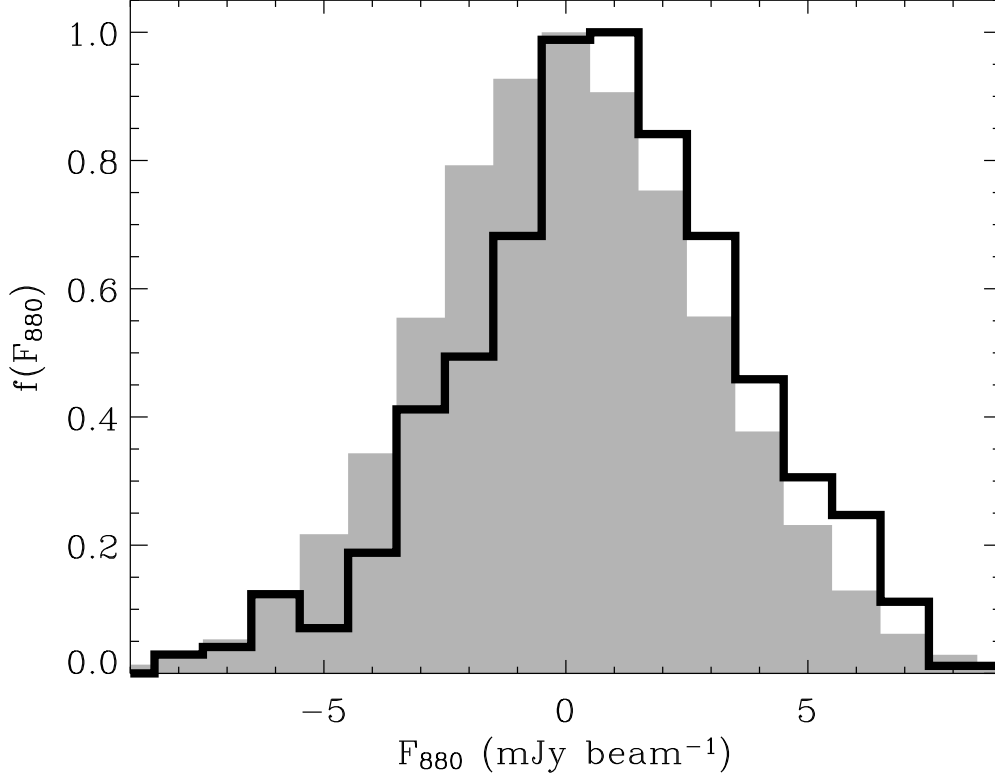


Figure 3: Normalized histograms of the flux distribution toward the undetected proplyds (line) and the rest of the map within the primary beam FWHM (grayscale). The five detected proplyds have not been included in either plot and the fluxes were not corrected for primary beam attenuation. The flux distribution toward the undetected proplyd positions is offset from the background flux distribution and has a mean value $0.8 \text{ mJy beam}^{-1}$.

TABLE 1
Masses of the detected propyds

Proplyd	$F_{880\mu\text{m}}^{\text{a}}$ (mJy)	peak S/N	Bremsstrahlung ^b (mJy)	M^{c} ($10^{-2}M_{\odot}$)
163–317	33.3	8.7	5.9	1.9
167–317 ^d	21.9	5.3	17.3	...
170–337	38.1	7.3	3.7	2.4
171–334	24.6	7.5	2.1	1.6
171–340	18.3	4.0	0	1.3

^a Observed flux, corrected for primary beam attenuation

^b Estimated contribution from ionized gas

^c $\kappa = 0.03 \text{ cm}^2 \text{ g}^{-1}$, $T = 20 \text{ K}$

^d $\theta^1 \text{ Ori G}$; no significant dust excess

TABLE 2
Proplyd properties

Proplyd	Dust excess?	Type ^a	D_* (10^{16} cm)	M_* (M_\odot)		R_D (AU)
				0.3 Myr	1 Myr	
163-317	✓		4.7	0.9	1.8	
170-337	✓	jet,od	10.9	1.1	2.2	40
171-334	✓		9.5	> 2.5	> 2.5	
171-340	✓	sd/e	12.9			40
157-323	×		7.4	1.0	2.1	
158-323	×		6.3	1.4	> 2.5	
158-326	×	sd/e	6.5	0.3	0.7	40
158-327	×	sd/e	7.2			20
159-338	×		11.9	0.1	0.2	< 20
160-328	×	od	11.1			45
161-314	×		5.1			
161-322	×		4.1			
161-324	×		4.2	< 0.1	< 0.1	
161-328	×	sd/e	5.1	0.1	0.1	40
163-322	×		2.0			
163-323	×		1.4	0.2	0.2	
166-316	×		4.9	0.3	0.8	< 20
167-317	×	jet	5.2	1.3	2.4	
168-326	×		4.2	0.1	0.1	
168-328	×		4.5	0.3	0.7	
169-338	×		11.1			
171-315	×		8.2			
176-325	×		11.0	0.4	0.9	

^a sd/e = silhouette disk in bright envelope, od=disk seen in O[I] emission